

Interacting dark energy collapse with matter components separation

M. Le Delliou^{a,b} and T. Barreiro^{c,d}

^aDepartamento de Física Matemática, Instituto de Física, Universidade de São Paulo, CP 66.318 — 05314-970, São Paulo, SP, Brasil

^bCentro de Astronomia e Astrofísica da Universidade de Lisboa, Faculdade de Ciências, Ed. C8, Campo Grande, 1769-016 Lisboa, Portugal

^cDepartamento de Matemática da FFMCC, Universidade Lusófona de Humanidades e Tecnologias, Campo Grande, 376 — 1749-024 Lisboa, Portugal

^dInstituto de Plasmas e Fusão Nuclear, Instituto Superior Técnico, Avenida Rovisco Pais, 1 — 1049-001 Lisboa, Portugal

E-mail: Morgan.LeDelliou@uam.es, delliou@cii.fc.ul.pt, tmbarreiro@ulusofona.pt

Abstract. We use the spherical collapse model of structure formation to investigate the separation in the collapse of uncoupled matter (essentially baryons) and coupled dark matter in an interacting dark energy scenario. Following the usual assumption of a single radius of collapse for all species, we show that we only need to evolve the uncoupled matter sector to obtain the evolution for all matter components. This gives us more information on the collapse with a simplified set of evolution equations compared with the usual approaches. We then apply these results to four quintessence potentials and show how we can discriminate between different quintessence models.

Keywords: dark matter simulations, dark energy theory, semi-analytic modelling

ArXiv ePrint: [0812.6373](https://arxiv.org/abs/0812.6373)

Contents

1	Introduction	1
2	The spherical collapse in interacting DM/DE quintessence models	3
2.1	Background evolution	3
2.1.1	Background Friedmann evolution	4
2.1.2	Energy density conservation equations	4
2.2	Choice of potential	5
2.2.1	Double exponential	5
2.2.2	Albrecht-Skordis	5
2.2.3	Steinhardt	6
2.2.4	SUGRA	6
2.3	Collapse evolution equations	6
2.3.1	Uncoupled collapse	6
2.3.2	Coupled collapse	7
2.3.3	Simplified evolution	7
2.3.4	Other assumptions	7
2.3.5	Non-linear evolution	8
2.3.6	Linear evolution	8
3	Numerical implementation and results: critical density evolution	9
3.1	Top hat and critical overdensity evolutions	9
3.1.1	Collapse of uncoupled matter/coupled DM	9
3.1.2	Relative linear overdensities evolution	10
3.1.3	Critical overdensities evolution	11
3.2	Critical overdensities dependence on coupling	13
3.2.1	General remarks	13
3.2.2	discriminating models	13
4	Discussion and conclusion	14
A	Unequal initial overdensities	15
B	Observational constraints	16
B.1	Supernovae	16
B.2	Cosmic Microwave Background	16
B.3	Results	17

1 Introduction

The field of cosmology, although receiving an accumulation of precision observations in the recent years and despite their consistence with the “concordance model”, Λ CDM, is yet to decide on the content of the universe. The wealth of data available ranges from large scale geometric assessments like the precise measurements of the Cosmic Microwave Background (CMB) [1], intermediate scale evaluations like Baryon Acoustic Oscillations (BAO) [2] and

more local scales measures of the Hubble constant (H_0) via observations of standard candles like Cepheid variable stars [3] or Type Ia Supernovae (SNIa) [4]. Although the simplicity of the concordance model would place it in a prominent position, given its compatibility with observations, it suffers from theoretical shortcomings that question our understanding of gravity and our knowledge of physics: the fine tuning problem and the coincidence problem (for a review, see [5]). Introduction of dynamical forms of dark energy (hereafter DE) was then considered to try and overcome those problems [5–7], and quintessence scalar fields [8–10] are the most obvious candidates (for review see [11]). However if they can overcome the first problem, the second remains in various forms. In this framework, DE and dark matter (DM) are the fundamental building blocks of the cosmological standard model based on general relativity, which leaves unknown and dark nearly 96% of the Universe’s energy content. Although coupling to baryonic matter is tightly constrained by local gravity tests [12], this undetermined aspect opens the door to all kinds of couplings within the dark sector, including non-linear DE self-gravitating clustering [13, 14] and non-minimal coupling between the two dark species, introduced either by ad hoc arguments [15] or because dark energy and dark matter are unified in the context of some framework [16–18]: the implications of interacting DE-DM on cosmological observations were examined in works such as [15, 19–22, and references therein], while analysis of CMB and BAO such as [23, 24], or of gamma-ray bursts as in [25], have constrained some coupled quintessence models. Studies have demonstrated that signatures of such coupled models can be found in the background expansion history of the universe and on cosmic structure formation, especially at larger, galaxy clusters, scales [26–30]. However, despite the naturalness of allowing dark sector interaction, a degeneracy exists between the various possible amounts of interacting DM at the homogeneous dynamical level [31], that only non-linear clustering properties might disentangle. Another consequence of interacting dark sector could be the violation of the Equivalence Principle: originating in the DE-DM interactions [32–42], this could be seen in differential DM-baryons tidal arms from disrupted satellite galaxies [32, 33, 39, 41], totally disrupted satellites like the bullet cluster [34] or DM caustics [42].

Dynamic DE impact on structure formation, in the form of a quintessence scalar field, was first restricted to linear or perturbation theory of structure evolution [43]. In the mildly non-linear regime, [44, 45] found the smallest scale of quintessence fluctuations are larger than the clusters scale, so this clustering should be negligible. Nevertheless, studies of the fully non-linear regime showed marked differences in DM structures between DE models that cluster and those that do not [13]. The clustering properties of DE models remain however an open question. Non-linear structure formation is traditionally studied with N-body simulations, as e.g. in [46, 47]. Insofar as investigating structure formation with DE, since no dynamical model seem preferred, the flexibility of semi-analytical methods have lead to numerous studies such as [13, 14, 45, 48–55]. The methods used, prevalent at the core of entirely semi-analytic galaxy formation models, i.e in [56–62], revolve around similar mass function-determining schemes as the methodology developed by Press & Schechter [63, hereafter PS]. The latter method uses a spherically symmetric dynamical model to relate the collapse of massive structures to a density threshold in the linearly extrapolated density field. In this way, it is possible to apply Gaussian statistics to the initial density field in order to count the numbers of collapsed structures above a given mass threshold at a particular epoch. The spherical collapse model [64–76] or its variants are therefore at the root of such approach.

Non-gravitational interactions is expected to impact significantly on the free fall of DM, whether it links baryons with DM [77] or originates in interacting DE [32–34, 39, 41, 42].

This investigation aims at revealing that impact in the spherical collapse model, as suggested in [35, 36], in its dependence on the DE model involved and on the difference between the collapses of coupled and uncoupled matter species, as mark of a baryon/DM segregation. For that purpose, we singled out a range of quintessence potentials and a range of interaction parameters to gauge their influence on the violation of the Equivalence Principle between coupled and uncoupled matter manifested by this segregation: the double exponential potential [78], the infinite sum of inverse power potential [79], the supergravity motivated potential (SUGRA) [80], and the superstring theory motivated potential of [81]. For these models, we used the spherical collapse model to obtain separately the uncoupled matter and DM overdensity parameters evolution and their critical values, arguably showing how the baryon/DM drift can manifest itself depending on the DE model. We introduced a novel approach, noticing that a single collapse radius kept for all species lead to algebraic relations between their overdensities. Thus we simplified the treatment of dynamics which entails following dust-like uncoupled matter in a DE environment. This simpler evolution manages to recover previous results such as [14, 55] and in the process allows to differentiate between coupled and uncoupled matter evolution.

The paper is organised as follows: in section 2, the evolution equations for both the baryons or uncoupled matter and for the coupled DM are detailed, followed by the forms of the potentials; section 3 presents our analysis of the segregated spherical collapse semi-analytical model. Finally, in section 4 we discuss the results and present our conclusions.

2 The spherical collapse in interacting DM/DE quintessence models

The spherical collapse model (pioneered in [64–68] and summarised in [69]) is a powerful tool of semianalytical methods to study gravitational clustering, e.g. [70–76], in particular with many different models of interacting DE as in [13, 14, 45, 48–55].

The DE models considered here are interacting quintessence dynamical scalar fields. The governing equations of motion come from Einstein’s field equations (Friedmann and Raychaudhuri equations) and Bianchi identities (fluids energy density conservations), for a multicomponent fluid with a top hat density model. The top hat model assumes a Friedmann-Lemaître-Robertson-Walker (FLRW) background and a higher curved FLRW spherical collapsing patch. In this paper we will always assume the background to be flat (no curvature). The multicomponent fluid comprises baryons, uncoupled DM, coupled DM and DE. We treat the baryons and uncoupled DM in a single uncoupled matter fluid. The Bianchi identities for each species reflect the coupling of DE as well as its clustering properties in the collapsing patch with heat fluxes. The scalar field obeys a corresponding Klein-Gordon equation. The type of quintessence is entirely determined by its potential, however an important part of the model, as far as structure formation is concerned, is given in the interaction parameter as well as the clustering parameter.

2.1 Background evolution

we will use the following notations

- energy densities:

ρ_ϕ for DE energy density (quintessence from a scalar field ϕ), ρ_m for total matter, ρ_u for uncoupled matter (including uncoupled DM and baryons) and ρ_c for coupled DM. These energy densities are related by

$$\rho_m = \rho_u + \rho_c, \quad (2.1)$$

where the uncoupled matter component includes the baryon and the uncoupled dark matter energy components,

$$\rho_u = \rho_b + \rho_{udm}. \quad (2.2)$$

For the total energy density, we use

$$\rho_{tot} = \rho_m + \rho_\phi. \quad (2.3)$$

- density parameters

we define the density parameter for each species as

$$\Omega_i = \frac{\rho_i}{\rho_{tot}}. \quad (2.4)$$

- FLRW Hubble parameter defined in terms of scale factor a :

$$H = \frac{1}{a} \frac{da}{dt} = \frac{\dot{a}}{a}, \quad (2.5)$$

2.1.1 Background Friedmann evolution

The Einstein field equations for the flat FLRW background are reduced to the Friedmann and Raychaudhuri equations for the background scale factor a

$$H^2 = \frac{\kappa^2}{3} (\rho_m + \rho_\phi) \quad \dot{H} + H^2 = -\frac{\kappa^2}{6} (\rho_m + \rho_\phi + 3P_\phi), \quad (2.6)$$

with P_ϕ being the pressure of the dark energy.

2.1.2 Energy density conservation equations

Aside from the Einstein equations, the conservation of each cosmic fluid component is governed by the corresponding Bianchi identity for the homogeneous FLRW model, so we have for the uncoupled, coupled matter and DE

$$\dot{\rho}_u + 3H\rho_u = 0, \quad \dot{\rho}_c + 3H\rho_c = \rho_c B' \dot{\phi}, \quad \dot{\rho}_\phi + 3H(\rho_\phi + P_\phi) = -\rho_c B' \dot{\phi}, \quad (2.7)$$

where the DE-DM interaction manifests in the heat fluxes $\Gamma_c = -\Gamma_\phi = \rho_c B' \dot{\phi}$, with $B' = \frac{dB(\phi)}{d\phi}$ the interaction rate. The first proposals for such a flux appeared in [15] with the choice of a constant B' . Other forms can be chosen, as, e.g., in [82], however we will concentrate here on the form $B' = -C\kappa$ with the free parameter C chosen appropriately ($C = 0$ representing of course absence of DE-DM coupling). Both matter conservation equations (2.7-a,b) can be integrated, yielding

$$\rho_u = \rho_0 \Omega_{u0} \left(\frac{a_0}{a}\right)^3, \quad \rho_c = \rho_0 \Omega_{c0} \left(\frac{a_0}{a}\right)^3 e^{B-B_0}, \quad (2.8)$$

where ρ_0 is the critical density at present, the subscript 0 denoting quantities at present, so $B_0 = B(\phi_0)$. Note that e^B can be interpreted as the mass of the coupled DM.

2.2 Choice of potential

We chose a range of potentials $V(\phi)$ likely to reflect a variety of DE behaviours. The double exponential potential is essentially a scaling model, like a single exponential potential, that is complemented by the second exponential to allow the scalar field to start dominating the energy density at present times. The Albrecht-Skordis potential is the only potential we use that has a local minimum, so that the present energy density for the scalar field is obtained through oscillations around this minimum. The Steinhardt and the SUGRA potentials are both typical tracking potentials. In appendix B we use the present SNeIa and CMB observations to constraint the coupling C we use in these models, where we can verify that the Steinhardt and the SUGRA potentials favor a non-zero value for the coupling parameter C , positive for the Steinhardt potential and negative for the SUGRA potential.

In this framework, the energy density and pressure of the scalar field are given by

$$\rho_\phi = \frac{\dot{\phi}^2}{2} + V(\phi), \quad P_\phi = \frac{\dot{\phi}^2}{2} - V(\phi). \quad (2.9)$$

They come into play in eq. (2.7-c) which is, for a scalar field, the Klein-Gordon equation

$$\ddot{\phi} + 3H\dot{\phi} + V' = -\rho_c B'. \quad (2.10)$$

2.2.1 Double exponential

The double exponential potential was introduced by [78] to build a more realistic DE candidate out of the two regimes of the single exponential potential [8, 83]: one which tend to dominate the energy density, the other which mimics the time evolution of the background. Originally, the simple exponential potential gets its motivation from its display of a generic form for moduli fields from extradimensional theories flat directions. Potentials of this type could arise in string theory from Kaluza-Klein type compactification [78]. The result is called double exponential potential (2EXP), which follows its name

$$V(\phi) = \Lambda_\phi^4 \left(e^{-\lambda_1 \phi} + e^{-\lambda_2 \phi} \right). \quad (2.11)$$

Throughout the rest of the paper all numerical evolutions for this potential are done with the parameter values $\lambda_1 = 20.5$ and $\lambda_2 = 0.5$. The value of Λ_ϕ is fine-tuned to achieve a present value of $\Omega_\phi = 0.7$.

2.2.2 Albrecht-Skordis

The combination of a single exponential with a phenomenologically inspired polynomial, motivated by superstring theory, introduced by [81] creates a local minimum in which the field can oscillate and get trapped. The parameters orders of magnitude are then more natural ($\sim O(M_{Pl})$) for a range where the model is able to satisfy a number of cosmological constraints and provide late time acceleration, however they still require fine tuning caused by the coincidence problem. It can take the form (AS)

$$V(\phi) = \Lambda_\phi e^{-\kappa\lambda\phi} \left[A + (\kappa\phi - B)^2 \right]. \quad (2.12)$$

The values of the parameters we used for our numerical evolutions were $A = 0.01$, $B = 33.96$ and $\lambda = 8$. Again, Λ_ϕ is fine-tuned to obtain $\Omega_\phi = 0.7$ at present.

2.2.3 Steinhardt

In [79], Steinhardt propose this new form of potential by taking the infinite sum of inverse power potentials that would stem from global SUSY considerations [84]. It exemplifies well the tracking properties, desirable for quintessence potentials to correlate the fine tuning problem to the coincidence problem and thus reduce the theoretical cosmological constant problems to one. It can be written as (SP)

$$V(\phi) = \Lambda_\phi^4 \left(e^{\frac{1}{\kappa\phi}} - 1 \right). \quad (2.13)$$

The Steinhardt potential has no extra free parameters and Λ_ϕ is fine-tuned to achieve $\Omega_\phi = 0.7$ at present.

2.2.4 SUGRA

[80] motivated this potential from supergravity models and null vacuum superpotential expectation value in the low energy approximation. It takes the form (SG)

$$V(\phi) = \frac{\Lambda_\phi^{4+\alpha_\phi}}{\phi^{\alpha_\phi}} e^{\kappa^2 \phi^2/2}. \quad (2.14)$$

For our numerical results we used $\alpha_\phi = 11$, and fine-tuned Λ_ϕ to achieve a value of $\Omega_\phi = 0.7$ at present.

2.3 Collapse evolution equations

The aim of this study is to extend the usual spherical collapse to follow separately the evolution of the coupled and uncoupled (including baryons) components of matter. The homogeneous degeneracy between those two components [31] is expected to be broken once we take into account their clustering properties. In the usual scenario, a FLRW flat background contains a central spherical patch, modeled as a positively curved FLRW with scale factor r . That scale factor is assimilated to the radius of the spherical patch [13, 14, 45, 48–55].

2.3.1 Uncoupled collapse

The collapsing uncoupled matter in this framework follows the conservation equation using the Hubble parameter $\mathcal{H} = \frac{\dot{r}}{r}$ in the collapsed patch,

$$\dot{\rho}_{u\star} + 3\mathcal{H}\rho_{u\star} = 0, \quad (2.15)$$

where henceforth we will denote with a \star subscript all collapsing quantities. This integrates to

$$\rho_{u\star} = \rho_{u\star i} \left(\frac{r_i}{r} \right)^3, \quad (2.16)$$

where the i subscript denotes values at some arbitrary initial time of collapse. Therefore the ratio of the uncoupled collapsed matter to its background (2.8-a) is then related to the radius through

$$\frac{\rho_{u\star}}{\rho_u} \propto \left(\frac{a}{r} \right)^3. \quad (2.17)$$

2.3.2 Coupled collapse

On the same token, the collapsing coupled DM follows the conservation equation

$$\dot{\rho}_{c\star} + 3\mathcal{H}\rho_{c\star} = \rho_{c\star} B'_\star \dot{\phi}_\star, \quad (2.18)$$

(with $B'_\star = B'(\phi_\star)$) which integrates to

$$\rho_{c\star} = \rho_{c\star i} \left(\frac{r_i}{r}\right)^3 e^{B_\star - B_{\star i}}, \quad (2.19)$$

and therefore the ratio of the coupled collapsed matter to its background (2.8-b) is also related to the radius through

$$\frac{\rho_{c\star}}{\rho_c} \propto \left(\frac{a}{r}\right)^3 e^{B_\star - B}. \quad (2.20)$$

2.3.3 Simplified evolution

Here we point out that this parallel evolution of coupled and uncoupled collapse relies heavily on the implicit assumption that all species collapse within the same radius, $r = r_c = r_u = r_\phi$. Introducing the definition of the energy density contrast,

$$1 + \delta_m = \frac{\rho_{m\star}}{\rho_m}, \quad 1 + \delta_u = \frac{\rho_{u\star}}{\rho_u}, \quad 1 + \delta_c = \frac{\rho_{c\star}}{\rho_c}, \quad (2.21)$$

one can rewrite the radius of spherical collapse (2.17) into

$$\left(\frac{a/a_i}{r/r_i}\right)^3 (1 + \delta_i) = 1 + \delta_u. \quad (2.22)$$

Without loss of generality, the parallel between eqs. (2.17) and (2.20), and the total matter, can be expressed in the relations

$$1 + \delta_c = (1 + \delta_u) \cdot e^{B_\star - B}, \quad 1 + \delta_m = (1 + \delta_u) \cdot \frac{\rho_{c0} e^{B_\star - B_0} + \rho_{u0}}{\rho_{c0} e^{B - B_0} + \rho_{u0}}. \quad (2.23)$$

However these relations assume the initial conditions for δ_c and δ_u to be the same. We relax in Appendix A this condition, showing that the final results are not significantly affected. For simplicity, we will keep assuming the equality of initial conditions for the rest of the paper, as is implicit in previous results [14, 53, 55].

We thus emphasize that the assumption, commonly made in the field of DE spherical collapse [13, 14, 45, 48–55], setting the same radius of collapse for all species ($r = r_c = r_u = r_\phi$), implies that all matter density contrasts are related to the uncoupled case and their dynamics can be obtained through that of the uncoupled matter. This simplifies greatly the treatment and governing equations previously used for coupled and collapsing DE spherical collapse, e.g. as in [14, 53, 55], since one only needs to evolve the uncoupled DM overdensity equations to get the coupled one via the above constraints. This means that we can concentrate on the evolution of the uncoupled matter, and recover the full evolution for all components.

2.3.4 Other assumptions

The central spherical patch is treated as a curvature varying Friedmann model with the Raychaudhuri equation while the background is a regular Friedmann model with lower density. The backreaction is neglected invoking the Birkhoff theorem, assuming some extension of it to cosmological backgrounds can be applied and the existence of a global separation shell [85–87] within the boundary between the two regions.

2.3.5 Non-linear evolution

We now will get the overdensity evolution equations for the uncoupled DM component since the algebraic relation with the coupled overdensity, from the unique radius constraint, renders the coupled evolution equations superfluous.

Using eq. (2.22), together with the Bianchi energy conservations (eqs. 2.7-a and 2.15) for the Hubble parameters of the background and collapsing regions yields the overdensity first derivative

$$\dot{\delta}_u = 3(1 + \delta_u)[H - \mathcal{H}]. \quad (2.24)$$

The Einstein field equations in this frame are reduced to the Friedmann and Raychaudhuri equations for the background scale factor a (eqs. 2.6) and the collapsing radius r :

$$\dot{\mathcal{H}} + \mathcal{H}^2 = -\frac{\kappa^2}{6} \sum (\rho + 3P)_\star, \quad (2.25)$$

to which the Klein-Gordon equations for the background (2.10) and collapsing region are added in the form, in the case of totally collapsing quintessence,

$$\ddot{\phi}_\star + 3\mathcal{H}\dot{\phi}_\star + V'_\star = -\rho_{c\star}B'_\star. \quad (2.26)$$

The case of the homogeneous quintessence obeys to the same equations except that in eq. (2.26), the collapsing Hubble parameter is replaced by that of the background. The overdensity evolution equation follows by differentiating eq. (2.24)

$$\left. \frac{\ddot{\delta}_u}{1 + \delta_u} - \frac{\dot{\delta}_u^2}{(1 + \delta_u)^2} \right|_u = 3 \left[\dot{H} - \dot{\mathcal{H}} \right]. \quad (2.27)$$

Eventually one gets, together with using eqs. (2.23-a, 2.25 and 2.6), (recall from it and from eq. 2.8-b that the coupled quantities are linked with the uncoupled ones)

$$\ddot{\delta}_u = -2\frac{\dot{a}}{a}\dot{\delta}_u + \frac{4}{3}\frac{\dot{\delta}_u^2}{1 + \delta_u} + \frac{\kappa^2}{2}(1 + \delta_u)[\delta_u\rho_u + \delta_c\rho_c] + \frac{\kappa^2}{2}[(\rho_{\phi_\star} + 3P_{\phi_\star}) - (\rho_\phi + 3P_\phi)](1 + \delta_u). \quad (2.28)$$

If we have no coupled matter, that is if $\rho_c = 0$, this is the usual equation for the evolution the spherical collapse of uncoupled matter as seen in [14]. Following this evolution of δ_u and using eq. (2.23-b) we can re-obtain the full matter evolution of [14].

2.3.6 Linear evolution

The linear evolution equations for the collapsing spherical patch starts from the quintessence field linearisation with $\phi_\star = \phi + \delta\phi$ of the Klein-Gordon eq. (2.26). We use the linearisation of eqs. (2.23)

$$\delta_{m,L} = \delta_{u,L} + \frac{\Omega_{c0}}{\Omega_{c0} + \Omega_{u0}e^{B_0 - B}}B'\delta\phi, \quad \delta_{c,L} = \delta_{u,L} + B'\delta\phi, \quad (2.29)$$

so we are left with the linear part of eq. (2.26)

$$\delta\ddot{\phi} + [3H + \rho_c B']\delta\dot{\phi} + [V'' + \rho_c\dot{\phi}B'']\delta\phi + \dot{\delta}_{u,L}\dot{\phi} + \delta_{c,L}\dot{\phi}B'\rho_c = 0. \quad (2.30)$$

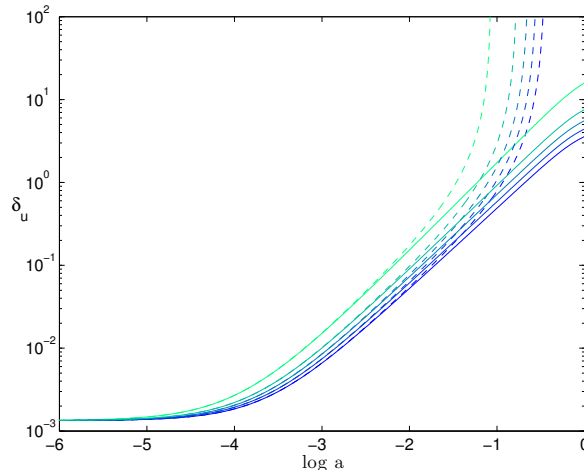


Figure 1. Spherical collapse evolution of the uncoupled matter for the inhomogeneous double exponential potential. We show both the linear (solid line) and the non-linear (dashed line) evolutions with $\Omega_u = 0.05$ and couplings $C = -0.2, -0.1, 0, 0.1$ and 0.2 from bottom to top.

The linearisation of the field source term of eq. (2.28) yields

$$[(\rho_{\phi_*} + 3P_{\phi_*}) - (\rho_\phi + 3P_\phi)]_L = 2 \left(2\dot{\phi}\delta\dot{\phi} - V'\delta\phi \right), \quad (2.31)$$

so the density evolution linearises as (again recall that eq. 2.29-b relates coupled and uncoupled overdensities)

$$\ddot{\delta}_{u,L} = -2\frac{\dot{a}}{a}\dot{\delta}_{u,L} + \kappa^2 \left[2\dot{\phi}\delta\dot{\phi} - V'\delta\phi \right] + \frac{\kappa^2}{2} [\delta_{u,L}\rho_u + \delta_{c,L}\rho_c]. \quad (2.32)$$

Again, if we have no coupled matter, this is the usual linear equation for the spherical collapse evolution of uncoupled matter as seen in [14]. Following this evolution of $\delta_{u,L}$ and using eq. (2.29-a) we can re-obtain the full matter linear evolution of [14].

3 Numerical implementation and results: critical density evolution

In order to follow the evolutions of the segregated uncoupled matter/DM spherical collapse for the four potentials we selected and inhomogeneous coupled DM to DE models, a matlab code was produced ad hoc. Here we present the results of our computations.

3.1 Top hat and critical overdensity evolutions

3.1.1 Collapse of uncoupled matter/coupled DM

To provide the reader with comparison points to previous works [13, 14, 45, 48–55], we present here the diagram of one example of time evolution for the linear and non-linear spherical top-hat collapse in a coupled inhomogeneous quintessence model. We make the arbitrary choice of using the double exponential potential, fixing the uncoupled matter to baryons, $\Omega_u = 0.05$, for a range of coupling $C \in [-0.2; 0.2]$. We display this plot of δ_u vs $\log a$ in figure 1. It shows that the linear values of overdensities go up with coupling, and consequently that the corresponding collapse time decreases, as expected [14, 53, 55]. This appears mainly as a consequence of

background evolution, as induced from eq. (2.8-b). The effect of inhomogeneous quintessence also speeds up collapse time, as seen in the last terms of eq. (2.28) or the second linear terms of eq. (2.32). This behaviour is similar for the other potentials and varying Ω_u with a fixed C gives the same or opposite behaviour depending on the sign of the chosen C (for more details on this $\Omega_u - C$ degeneracy, see section 3.1.3).

Note that the effect of the coupling parameter C on the evolution of the coupled matter energy density comes through term $e^{-C\kappa\Delta\phi}$, as seen in eq. (2.8), so that the effect comes through a combination of the parameter C and the range of the scalar field ϕ evolution. This means that the same value of the coupling parameter C can have different effects depending on the type of scalar potential used. For the four potentials we use, the range of the scalar field between matter-radiation equality and the present is approximately $\Delta\phi = 1.6$, $\Delta\phi = 1.8$, $\Delta\phi = 2.7$ and $\Delta\phi = 1.5$ for the two exponentials, Albrecht-Skordis, SUGRA and Steinhardt potentials respectively. We thus expect that the coupling strength is roughly equivalent between our four potentials, though slightly enhanced for the SUGRA potential. Note that the value of $\Delta\phi$ will also depend on the amount of coupling used, the quotes are for the mean of the evolutions we used numerically.

3.1.2 Relative linear overdensities evolution

As we have followed separately the coupled (DM) and uncoupled (including baryons) matter components, as opposed to previous works [14, 53, 55], it is interesting to confront all the models used in their relative linear overdensity evolution with respect to the uncoupled component. Note that although we are able to reproduce the results from [14, 53, 55], (a) we do so in a much simpler way as described in section 2.3.3, and (b) we focus on the coupled/uncoupled matter differences which are not discussed in those previous works. In figure 2, we display the evolutions of the coupled and total overdensities relative to the uncoupled one, for the models involving the four potentials described in section 2.2 in the tracking regime, and for a range of coupling. Again, we fix the uncoupled matter to baryons, $\Omega_u = 0.05$, for a range of coupling $C \in [-0.2; 0.2]$ for each model.

In all cases, absence of coupling makes all species behave the same way (we see, as expected, an horizontal line). Because the total overdensity combines coupled and uncoupled ones, as from eqs. (2.21)

$$\frac{\delta_m}{\delta_u} = \frac{\delta_c}{\delta_u} + \frac{\rho_u}{\rho_m} \left(1 - \frac{\delta_c}{\delta_u} \right), \quad (3.1)$$

we see that its departure from δ_u is always less than that of δ_c . This departure is small when varying C , however in the range of chosen variations, it appears markedly smaller for δ_m than for δ_c . In other words, for $C > 0$ we have $\delta_c < \delta_m < \delta_u$, while for $C < 0$ we have $\delta_c > \delta_m > \delta_u$. Negative couplings, with the form of eq. (2.7-b) and $B' = -C\kappa$, seem to induce stronger collapse in the coupled DM than in the uncoupled matter, whereas positive couplings have the opposite effect, although with a much stronger discrepancy than for the negative couplings in all models. This can also be interpreted from eq. (2.23-a) as $\phi_* - \phi > 0$. The qualitative behaviour for the double exponential, Steinhardt and SUGRA potentials is quite regular. However the Albrecht-Skordis potential displays quite strong oscillations in the linear overdensity near late times, reflecting its nature driving the field towards its local minimum around which it oscillates. This will be discussed further in section 3.2.

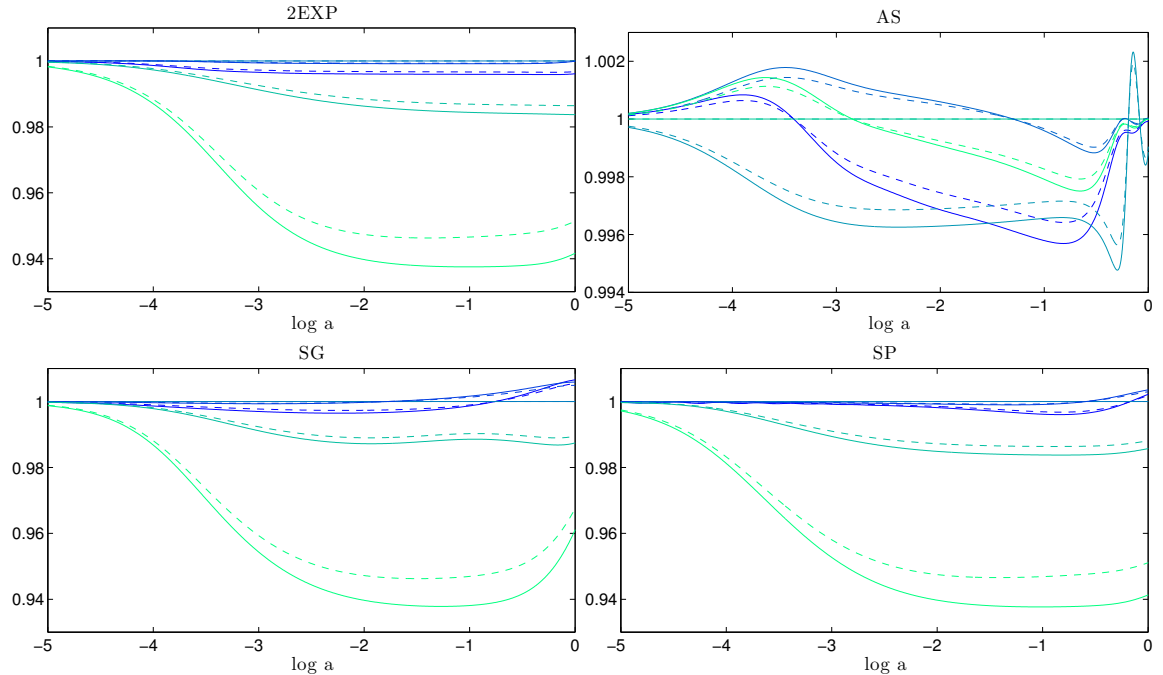


Figure 2. Relative linear overdensity evolution for $\delta_{c^*,L}/\delta_{u^*,L}$ (solid line) and $\delta_{m^*,L}/\delta_{u^*,L}$ (dashed line), for the potentials: double exponential (2EXP), Steinhardt (SP), SUGRA (SG), Albrecht-Skordis (AS). The values of coupling are $C = -0.2, -0.1, 0, 0.1$ and 0.2 (dark to light) for all the potentials except Albrecht-Skordis where $C = -0.2, -0.1, 0$ and 0.05 .

3.1.3 Critical overdensities evolution

We now present the diagrams of critical overdensities as a function of their collapse redshift for the four potentials. This time again, we fix the uncoupled matter to baryons, $\Omega_u = 0.05$, for a range of coupling $C \in [-0.2; 0.2]$ for each model.

Note that it can be shown that fixing the coupling respectively to a positive or negative value, for a range of uncoupled matter parameter $\Omega_u \in [0.05; 0.3]$ can mimic the effect of varying the coupling. The interval is chosen such that the lower limit restricts uncoupled matter to measured baryons, while the upper limit corresponds to no coupled matter (recall that we fix $\Omega_m = \Omega_u + \Omega_c = 0.3$). With such parameterisation, growing Ω_u is indirectly equivalent to decreasing the amount of coupling $|C|$. Thus varying Ω_u can be mapped to varying C , accounting for the sign of the constant C chosen. This behaviour seems to extend the dark degeneracy found at the homogeneous level [31]. However, the spatial segregation between the coupled and uncoupled matter components illustrated in the overdensities opens the door for mass determinations of each component separately, if the segregation is clear enough. Moreover, studies such as [35–38, 40] access directly the value of the coupling through the virial ratio of clusters, so that degeneracy should, in principle, be broken.

In figure 3, the leftmost panels give the homogeneous quintessence models behaviour while the rightmost panels recall the total matter (dashed line) collapse of the inhomogeneous coupled model for comparison with previous works [13, 14, 53, 55]. These panels also provide the uncoupled (dotted) and coupled (solid) evolutions. The scale and range of the diagrams is kept for each panel within a row for comparison purpose.

As is now known [14, 53, 55], the variations induced by turning on coupling in homo-

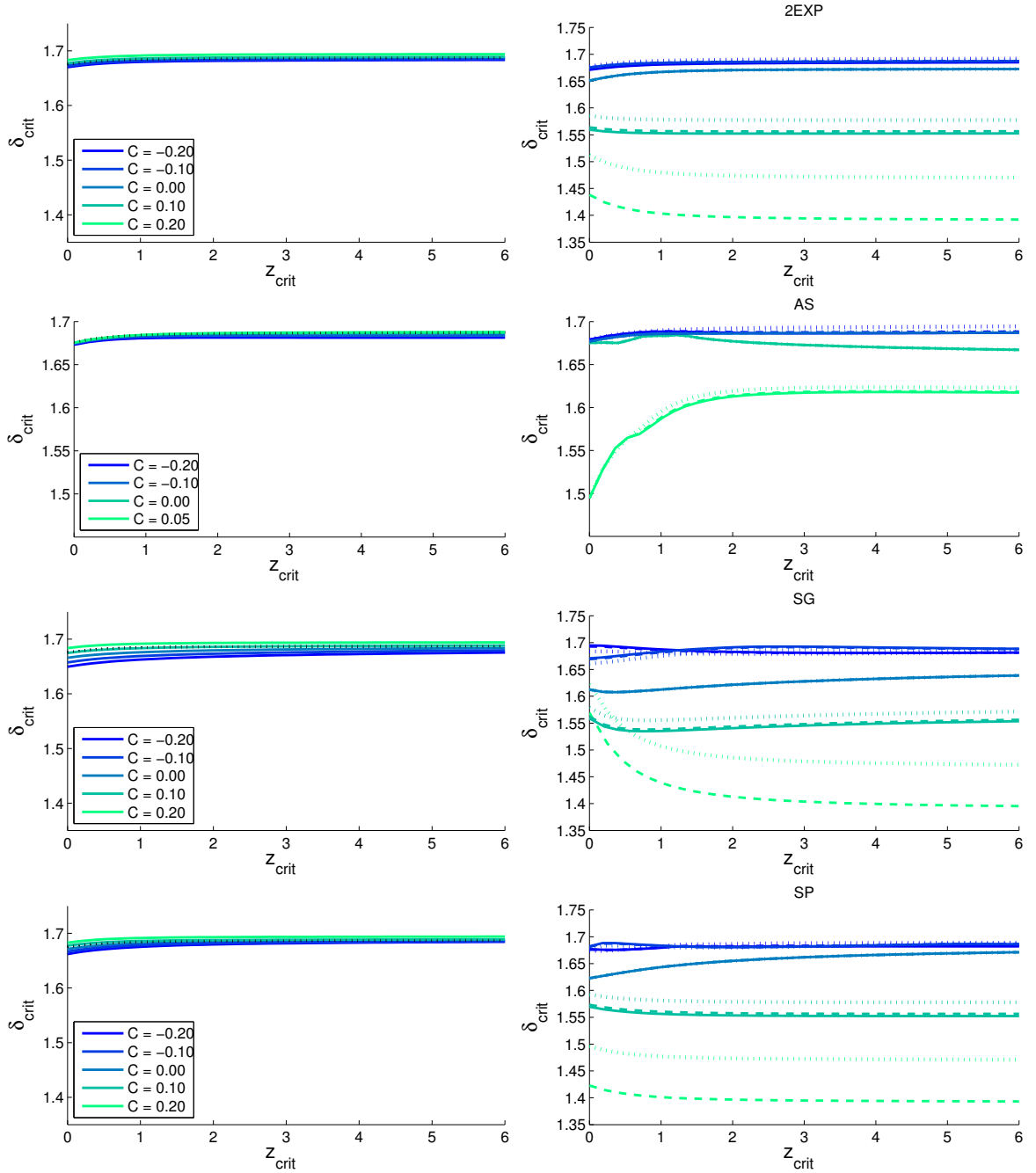


Figure 3. Critical overdensities as a function of the non-linear collapse redshift for the double exponential (2EXP), Albrecht-Skordis (AS), SUGRA (SG) and Steinhardt (SP) potentials. The left panel represents a homogeneous quintessence model with the total matter density contrast (solid lines) and as a reference the Λ CDM result (dotted line). The right panel represents an inhomogeneous quintessence model, with the density contrasts for uncoupled matter (dotted line), coupled matter (solid line) and total matter (dashed line). The curves lightness reflect the values of C .

geneous quintessence are markedly smaller than that induced in collapsing models (compare left and right, dashed lines, panels). Similarly as seen in figure 1, increasing the value of C

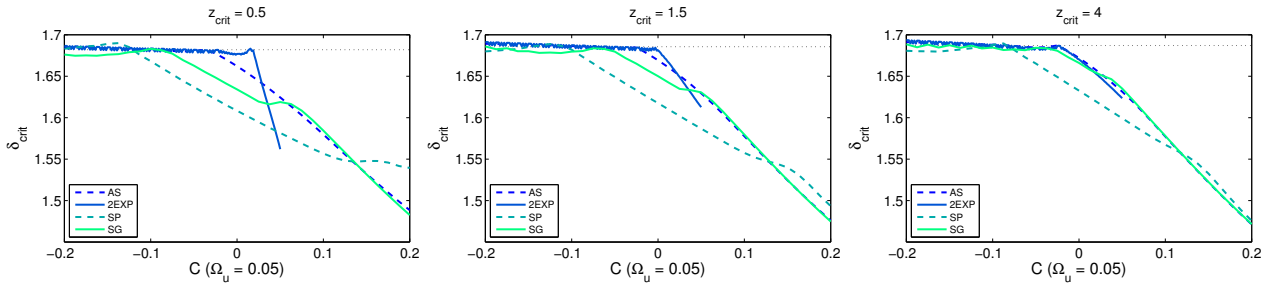


Figure 4. Value of the uncoupled matter critical overdensity as a function of the coupling at a reference critical redshift of $z = 0.5$, $z = 1.5$ and $z = 4$. We use $\Omega_u = 0.05$. Each panel shows the results for the four potentials we study, from bottom to top: SUGRA, Steinhardt, double exponential and Albrecht-Skordis. The dotted line shows the critical overdensity value at the reference redshift in a Λ CDM model.

both increase the corresponding value of critical linear overdensity and the collapse redshift.

Thanks to the simplifying assumption that leads to eqs. (2.23), the dynamics needs only to be followed in $\delta_{u,crit.}$, shown in the right panel. It displays, in the negative coupling range, a lower collapse threshold $\delta_{u,crit.}$ for uncoupled matter than for coupled DM, consistent with eq. (3.1), with a sharper decrease towards later times for uncoupled matter. The picture is inverted in the positive coupling range: the DM collapse threshold $\delta_{c,crit.}$ is lower than for uncoupled matter in that case and the increase towards later times is sharper than for uncoupled matter. This vindicates the claim for baryon-DM segregation with coupled DE.

3.2 Critical overdensities dependence on coupling

3.2.1 General remarks

We synthesise our results for all the potentials in figure 4, representing their variations in critical overdensities as a function of coupling.

Note that the features of each potential in figure 4 agree with those of figure 3. Those features seems to characterise each potential.

A striking first observation is that, at fixed time ($z_{crit.}$), the critical overdensities generally are decreasing with C , in agreement with section 3.1.3's considerations. This can be understood as fixing $z_{crit.}$ requires to vary initial δ_i to maintain that collapse time so as to compensate the effect of the variations of C in the exact opposite way. From figure 1, increased C leads to decreased collapse time, so a smaller initial δ_i is required to compensate that effect, leading to a smaller final linear overdensity.

Recall from section 3.1.3 that increasing Ω_u decreases the amount of coupling $|C|$. In particular, the curve features found for SP, AS, 2EXP and SG in the respective $C > 0$ and $C < 0$ ranges of the panels can be mapped in corresponding varying Ω_u diagrams.

3.2.2 discriminating models

For larger values of z all potential behave similarly while at smaller redshifts, each potential displays individual features due to the emergence of DE dominated behaviour.

The 2EXP potential displays sections, mostly in the $C > 0$ part, where it also behaves linearly, with a larger slope than the SG. This can be conjectured as reflecting the scaling solution behaviour. However it has an hybrid behaviour as its critical overdensity asymptotes

to a constant (the Λ CDM critical overdensity) in the $C < 0$ region. That behaviour can be attributed to oscillations around its dominating solution.

The SP and SG potentials offer the most features: they match the 2EXP linear $C > 0$ behaviour as well as its more or less constant Λ CDM asymptote $C < 0$ region at large $|C|$ but shows an intermediate region with similar slope. One can conjecture a link between them, both potentials being built from inverse powers: the SG, with an exponential cutoff, the SP, of an infinite sum of inverse powers.

Finally, the AS potential brings the most untypical features: it doesn't admit solutions for $C > 0.05$ and it decreases faster than any other model for $C > 0$. Whereas for $C < 0$ it oscillates and asymptotes to a constant Λ CDM value, like the 2EXP potential. This can be interpreted from the fact that the AS potential offers a local minimum for the field to be trapped in and oscillate around. From eqs. (2.7-b,c), we see that $C > 0$ feeds more energy in the DE sector (assuming DE slow roll so $\dot{\phi} > 0$ as all chosen potentials decay with field, in a first approximation), thus feeding the oscillations, whereas $C < 0$ has the opposite energy transfer and thus dampens the oscillations around the potential local minimum, where the model effectively behaves like a cosmological constant. Thus similarly as with 2EXP but in a stronger way, as the oscillation behaviour is stronger in AS than 2EXP, we have the dampened behaviour in the constant asymptote region and the excited behaviour in the negative slope region.

Of course this requires deeper investigations.

4 Discussion and conclusion

In this work we have presented results supporting the segregation of uncoupled matter and coupled DM in interacting DE models and have done so with the exposition of an innovative and simplifying approach to the dynamics of such system. The method employed relies on the assumption common in the field that all species collapse within the same top hat radius. The novel treatment comes from relying on the algebraic relations between species overdensities derived from that assumption to reduce the need to follow complex dynamics of the collapse to the simpler evolution of uncoupled matter. This also clarifies the reason why most of the effects we found are mainly driven by background behaviours, principal components in the evolution equation outside of the uncoupled overdensity. Exploring the segregated spherical collapse, we made contact with previous work and established, in this model, the difference in behaviour between uncoupled matter and DM interacting with DE from (a) the differences in linear overdensity evolution between species, (b) the differences in critical overdensity functions between species, and (c) an original synthesis of critical overdensity as a function of coupling, directly or indirectly. On a smaller note, we also established the equivalence between variations of the coupling and variations of the amount of uncoupled DM. This degeneracy is reminiscent of [31] and possibly arising from the constraint of equal radii for all species. We expect it to be broken by (a) independent mass determination of the uncoupled and coupled components with clear enough segregation as argued in [41], and (b) direct coupling evaluation as in virial cluster studies [35–38, 40]. In the interaction model we chose, positive coupling corresponds to feeding the DE sector from the coupled DM density whereas negative coupling induces the opposite. This is a cornerstone to understand (a) that negatively coupled DM collapses more than uncoupled matter while the opposite is true of positively coupled DM; (b) that instabilities in the behaviour of some of the chosen potentials are enhanced by positively coupled DM collapse while the negatively coupled DM dampens them. This confirms the

potential detectability of dark sector coupling in a similar fashion as from the tidal streams of stars in the Sagittarius dwarf galaxy due to DM segregation [32, 33, 39, 41], or from caustics of DM [42], in this case with a distinct halo collapse threshold between baryons and coupled matter. Finally, it is possible to discriminate between potentials in their response to the amount of coupling. Those behaviours certainly are calling for further investigations.

Acknowledgments

The authors would like to thank Nelson Nunes for discussions. TB wishes to thank Orfeu Bertolami. MLeD also wishes to thank David Mota, for discussions and transmission of a MATLAB code and José Pedro Mimoso for many years of support through this project. It also involved the support CSIC (Spain) under the contract JAEDoc072, with partial support from CICYT project FPA2006-05807, at the IFT, Universidad Autonoma de Madrid, Spain. The work of M.Le D. is now supported by FAPESP (Brazil), with process number 2011/24089-5, at the DFMA/IF, Universidade de São Paulo, Brazil.

A Unequal initial overdensities

In section 2.3.3, we assumed that the initial values for the overdensities in coupled and uncoupled matter were equal, as in and most works in the field, like [13, 14, 45, 48–55]. It is however possible to keep independent the overdensity of each species. In particular, the coupled to uncoupled overdensity relation reads in general

$$1 + \delta_c = (1 + \delta_u) \frac{1 + \delta_{ci}}{1 + \delta_{ui}} \frac{e^{B_\star - B}}{e^{B_\star i - B_i}} = (1 + \delta_u) \Delta e^{B_\star - B}, \quad (\text{A.1})$$

defining $\Delta = \frac{1 + \delta_{ci}}{(1 + \delta_{ui}) e^{B_\star i - B_i}}$, such that the assumptions of equal matter ($\delta_{ci} = \delta_{ui}$) and zero quintessence initial overdensities ($\phi_{\star i} = \phi_i$) reduce to $\Delta = 1$, and thus eq. (A.1) simplifies into relation (2.23-a) used in section 2.3.3. For the total matter relation (2.23-b), the freedom transcribes as

$$\begin{aligned} 1 + \delta_m &= (1 + \delta_u) \frac{\rho_u}{\rho_m} + (1 + \delta_c) \frac{\rho_c}{\rho_m} = \frac{1 + \delta_u}{\rho_m} (\rho_u + \rho_c \Delta e^{B_\star - B}) \\ &= (1 + \delta_u) \cdot \frac{\Omega_{c0} \Delta e^{B_\star - B_0} + \Omega_{u0}}{\Omega_{c0} e^{B - B_0} + \Omega_{u0}}, \end{aligned} \quad (\text{A.2})$$

which again simplifies when $\Delta = 1$. The linear versions of eqs. (A.1) and (A.2) then read as

$$\delta_{c,L} = \delta_{u,L} + B' \delta \phi + \delta_{ci} - \delta_{ui} - B'_i \delta \phi_i, \quad \delta_{m,L} = \delta_{u,L} + \left(\frac{B' \delta \phi + \delta_{ci} - \delta_{ui} - B'_i \delta \phi_i}{1 + \frac{\Omega_{u0}}{\Omega_{c0}} e^{B_0 - B}} \right). \quad (\text{A.3})$$

The coupled overdensity equation can then be used, together with its non-linear counterparts, in the correspondingly modified scheme formed after eqs. (2.26), (2.32), (2.30) and (2.32) to follow the uncoupled evolution. Then, the coupled values can be transcribed algebraically from the uncoupled values. Since δ_{ci} and δ_{ui} are small, $\Delta \simeq 1$. As the differences in evolution are small and do not bring further light into the question of the segregated spherical collapse, we only present in the main paper the results for $\Delta = 1$.

B Observational constraints

B.1 Supernovae

We use the updated Union2.1 compilation from the Supernova Cosmology Project, consisting of a sample of 580 SNeIa [88]. We constrain our model through fitting the distance modulus $\mu(z)$,

$$\mu(z) = 5 \log_{10} (d_L(z)) + \mu_0 \quad (\text{B.1})$$

where $\mu_0 = M_B - 5 \log_{10} h$, with M_B representing the absolute magnitude of the SNeIa and h being the Hubble parameter at present in units of $100 \text{ km s}^{-1} \text{ Mpc}^{-1}$.

The luminosity distance $d_L(z)$ can be computed through

$$d_L(z) = (1+z) \int_0^z \frac{H_0}{H(z')} dz' \quad (\text{B.2})$$

The χ^2 to fit the data is then given by

$$\chi_{SN}^2 = \sum_{j=1}^{580} \frac{(\mu(z_j) - \mu_{obs,j})^2}{\sigma_{\mu,j}^2} \quad (\text{B.3})$$

with $\mu_{obs,j}$ and $\sigma_{\mu,j}$ being the observed distance modulus and its error for each supernova. We then marginalize this over the absolute magnitude M_B to obtain our final results (see for example [89, 90] for details).

B.2 Cosmic Microwave Background

A simple but effective CMB constraint for our models can be obtained from the shift R parameter as given in the WMAP collaboration 7 year results [1]. The shift parameter [91] is given by

$$R = \frac{\sqrt{\Omega_{m0}}}{1+z_d} d_L(z_d) \quad (\text{B.4})$$

with d_L being the luminosity distance B.2 and z_d the redshift at decoupling. We compute the value of z_d using the standard fitting formula from [92]. We also need the acoustic scale at decoupling,

$$l_A = \pi \frac{d_L(z_d)}{(1+z_d)r_s(z_d)} \quad (\text{B.5})$$

where r_s is the comoving sound horizon size at decoupling,

$$r_s(z_d) = \int_{z_d}^{\infty} \frac{1}{H(z) \sqrt{3 + \frac{9\rho_b}{4\rho_\gamma}}} dz \quad (\text{B.6})$$

with ρ_b and ρ_γ being respectively the baryons and photons energy density.

The χ^2 is then given by

$$\chi_{CMB}^2 = (\vec{x} - \vec{x}_{obs})^T C^{-1} (\vec{x} - \vec{x}_{obs}) \quad (\text{B.7})$$

where $\vec{x} = (l_A, R, z_d)$ and C^{-1} is the inverse covariance matrix from the observations. From WMAP7 we get

$$\vec{x}_{obs} = (302.09; 1.725; 1091.3) \quad (\text{B.8})$$

and

$$C^{-1} = \begin{bmatrix} 2.305 & 29.698 & -1.333 \\ 29.698 & 6825.270 & -113.180 \\ -1.333 & -113.180 & 3.414 \end{bmatrix} \quad (\text{B.9})$$

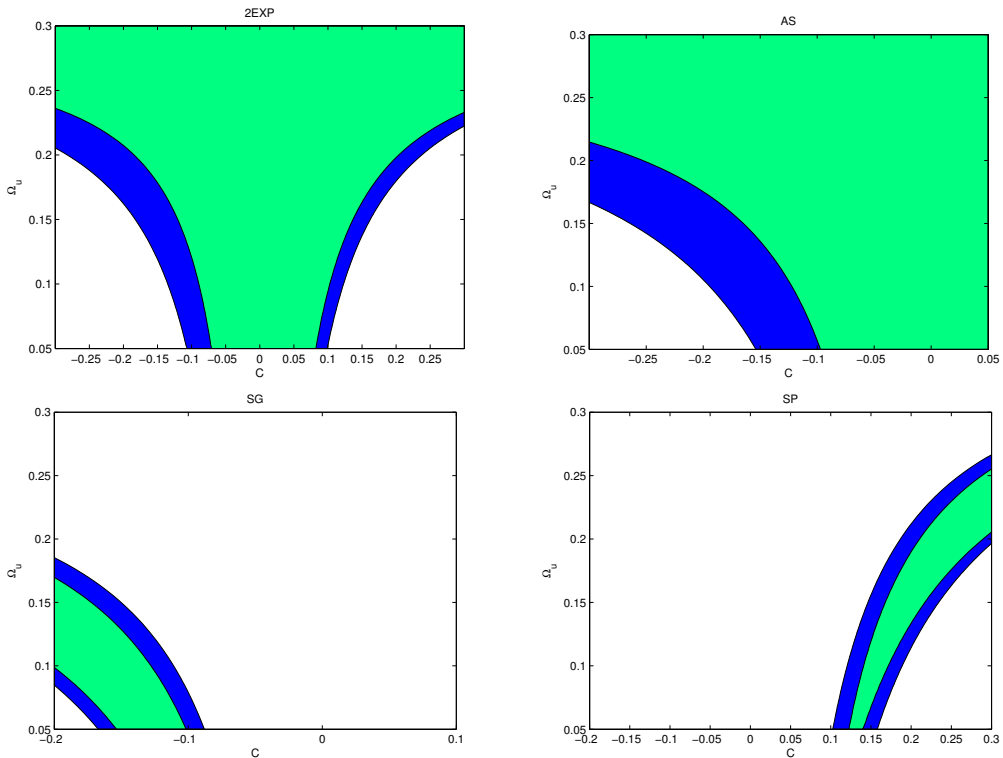


Figure 5. Two dimensional χ^2 likelihood for the double exponential (2EXP), Albrecht-Skordis (AS), SUGRA (SG) and Steinhardt (SP) potentials. We show the 68% and 90% confidence levels.

B.3 Results

We fixed all our parameters except the value of the coupling C and the amount of uncoupled dark matter Ω_u . That is, we fix the amount of coupled dark matter to be $\Omega_c = 0.3 - \Omega_u$, where $\Omega_u = \Omega_b + \Omega_{udm}$ includes both the baryons and the uncoupled dark matter components. The results for both constraints can be seen in Figure 5. We can see that present data favors negative values of C for the SUGRA potential and positive values of C for the Steinhardt potential, ruling out a scenario of uncoupled dark matter for these potentials. Consider, however, that these are just indicative results for the values of the parameters we use in this paper, and is not a full scale fit of the cosmological parameters for these models.

Fixing the value of $\Omega_u = 0.05$, we obtain as the best fit for the coupling C the values $C = 0.01 \pm 0.05$, $C = 0.01^{+0.06}_{-0.04}$, $C = -0.13 \pm 0.02$ and $C = 0.13 \pm 0.02$ for the double exponential, Albert-Skordis, SUGRA and Steinhardt potentials respectively.

References

- [1] **WMAP Collaboration** Collaboration, E. Komatsu et al., *Seven-Year Wilkinson Microwave Anisotropy Probe (WMAP) Observations: Cosmological Interpretation*, *Astrophys.J.Suppl.* **192** (2011) 18, [[arXiv:1001.4538](https://arxiv.org/abs/1001.4538)].
- [2] H. Lampeitl, R. Nichol, H. Seo, T. Giannantonio, C. Shapiro, et al., *First-year Sloan Digital Sky Survey-II (SDSS-II) supernova results: consistency and constraints with other intermediate-redshift datasets*, *Mon.Not.Roy.Astron.Soc.* **401** (2009) 2331–2342, [[arXiv:0910.2193](https://arxiv.org/abs/0910.2193)].

- [3] A. G. Riess, L. Macri, S. Casertano, M. Sosey, H. Lampeitl, et al., *A Redetermination of the Hubble Constant with the Hubble Space Telescope from a Differential Distance Ladder*, *Astrophys.J.* **699** (2009) 539–563, [[arXiv:0905.0695](#)].
- [4] **Supernova Cosmology Project** Collaboration, M. Kowalski et al., *Improved Cosmological Constraints from New, Old and Combined Supernova Datasets*, *Astrophys.J.* **686** (2008) 749–778, [[arXiv:0804.4142](#)].
- [5] S. M. Carroll, *The Cosmological constant*, *Living Rev.Rel.* **4** (2001) 1, [[astro-ph/0004075](#)].
- [6] V. Sahni and A. A. Starobinsky, *The Case for a positive cosmological Lambda term*, *Int.J.Mod.Phys.* **D9** (2000) 373–444, [[astro-ph/9904398](#)].
- [7] T. Padmanabhan, *Dark energy: The Cosmological challenge of the millennium*, *Curr.Sci.* **88** (2005) 1057, [[astro-ph/0411044](#)].
- [8] C. Wetterich, *Cosmology and the Fate of Dilatation Symmetry*, *Nucl.Phys.* **B302** (1988) 668.
- [9] B. Ratra and P. Peebles, *Cosmological Consequences of a Rolling Homogeneous Scalar Field*, *Phys.Rev.* **D37** (1988) 3406.
- [10] C. Wetterich, *The Cosmon model for an asymptotically vanishing time dependent cosmological 'constant'*, *Astron.Astrophys.* **301** (1995) 321–328, [[hep-th/9408025](#)].
- [11] E. J. Copeland, M. Sami, and S. Tsujikawa, *Dynamics of dark energy*, *Int.J.Mod.Phys.* **D15** (2006) 1753–1936, [[hep-th/0603057](#)].
- [12] S. M. Carroll, *Quintessence and the rest of the world*, *Phys.Rev.Lett.* **81** (1998) 3067–3070, [[astro-ph/9806099](#)].
- [13] D. Mota and C. van de Bruck, *On the Spherical collapse model in dark energy cosmologies*, *Astron.Astrophys.* **421** (2004) 71–81, [[astro-ph/0401504](#)].
- [14] N. J. Nunes and D. Mota, *Structure formation in inhomogeneous dark energy models*, *Mon.Not.Roy.Astron.Soc.* **368** (2006) 751–758, [[astro-ph/0409481](#)].
- [15] L. Amendola, *Coupled quintessence*, *Phys.Rev.* **D62** (2000) 043511, [[astro-ph/9908023](#)].
- [16] A. Y. Kamenshchik, U. Moschella, and V. Pasquier, *An Alternative to quintessence*, *Phys.Lett.* **B511** (2001) 265–268, [[gr-qc/0103004](#)].
- [17] M. Bento, O. Bertolami, and A. Sen, *Generalized Chaplygin gas, accelerated expansion and dark energy matter unification*, *Phys.Rev.* **D66** (2002) 043507, [[gr-qc/0202064](#)].
- [18] O. Bertolami and R. Rosenfeld, *The Higgs portal and an unified model for dark energy and dark matter*, *Int.J.Mod.Phys.* **A23** (2008) 4817–4827, [[arXiv:0708.1784](#)].
- [19] L. Amendola, *Linear and non-linear perturbations in dark energy models*, *Phys.Rev.* **D69** (2004) 103524, [[astro-ph/0311175](#)].
- [20] V. Pettorino and C. Baccigalupi, *Coupled and Extended Quintessence: theoretical differences and structure formation*, *Phys.Rev.* **D77** (2008) 103003, [[arXiv:0802.1086](#)].
- [21] A. Brookfield, C. van de Bruck, and L. M. Hall, *New interactions in the dark sector mediated by dark energy*, *Phys.Rev.* **D77** (2008) 043006, [[arXiv:0709.2297](#)].
- [22] R. Rosenfeld, *Reconstruction of interacting dark energy models from parameterizations*, *Phys.Rev.* **D75** (2007) 083509, [[astro-ph/0701213](#)].
- [23] L. Amendola, G. Camargo Campos, and R. Rosenfeld, *Consequences of dark matter-dark energy interaction on cosmological parameters derived from SNIa data*, *Phys.Rev.* **D75** (2007) 083506, [[astro-ph/0610806](#)].
- [24] R. Bean, E. E. Flanagan, I. Laszlo, and M. Trodden, *Constraining Interactions in Cosmology's Dark Sector*, *Phys.Rev.* **D78** (2008) 123514, [[arXiv:0808.1105](#)].

- [25] T. Barreiro, O. Bertolami, and P. Torres, *Gamma-Ray Bursts and Dark Energy - Dark Matter interaction*, *Mon.Not.Roy.Astron.Soc.* **409** (2010) 750–754, [[arXiv:1004.4562](#)].
- [26] M. Baldi, V. Pettorino, G. Robbers, and V. Springel, *Hydrodynamical N-body simulations of coupled dark energy cosmologies*, *Mon.Not.Roy.Astron.Soc.* **403** (2010) 1684–1702, [[arXiv:0812.3901](#)].
- [27] M. Baldi, *Time dependent couplings in the dark sector: from background evolution to nonlinear structure formation*, *Mon.Not.Roy.Astron.Soc.* **411** (2011) 1077, [[arXiv:1005.2188](#)].
- [28] R. Mainini and S. Bonometto, *Mass functions in coupled Dark Energy models*, *Phys.Rev.* **D74** (2006) 043504, [[astro-ph/0605621](#)].
- [29] P. Sutter and P. Ricker, *Detecting dark matter-dark energy coupling with the halo mass function*, [arXiv:0804.4172](#).
- [30] A. V. Maccio, C. Quercellini, R. Mainini, L. Amendola, and S. A. Bonometto, *N-body simulations for coupled dark energy: Halo mass function and density profiles*, *Phys.Rev.* **D69** (2004) 123516, [[astro-ph/0309671](#)].
- [31] M. Kunz, *The dark degeneracy: On the number and nature of dark components*, *Phys.Rev.* **D80** (2009) 123001, [[astro-ph/0702615](#)].
- [32] M. Kesden and M. Kamionkowski, *Tidal Tails Test the Equivalence Principle in the Dark Sector*, *Phys.Rev.* **D74** (2006) 083007, [[astro-ph/0608095](#)].
- [33] M. Kesden and M. Kamionkowski, *Galilean Equivalence for Galactic Dark Matter*, *Phys.Rev.Lett.* **97** (2006) 131303, [[astro-ph/0606566](#)].
- [34] G. R. Farrar and R. A. Rosen, *A New Force in the Dark Sector?*, *Phys.Rev.Lett.* **98** (2007) 171302, [[astro-ph/0610298](#)].
- [35] O. Bertolami, F. Gil Pedro, and M. Le Delliou, *Dark Energy-Dark Matter Interaction and the Violation of the Equivalence Principle from the Abell Cluster A586*, *Phys.Lett.* **B654** (2007) 165–169, [[astro-ph/0703462](#)].
- [36] O. Bertolami, F. G. Pedro, and M. Le Delliou, *The Abell Cluster A586 and the Equivalence Principle*, *Gen.Rel.Grav.* **41** (2009) 2839–2846, [[arXiv:0705.3118](#)].
- [37] O. Bertolami, F. G. Pedro, and M. L. Delliou, *Testing the interaction of dark energy to dark matter through the analysis of virial relaxation of clusters Abell Clusters A586 and A1689 using realistic density profiles*, *Gen.Rel.Grav.* **44** (2012) 1073–1088, [[arXiv:1105.3033](#)].
- [38] E. Abdalla, L. R. W. Abramo, J. Sodre, L., and B. Wang, *Signature of the interaction between dark energy and dark matter in galaxy clusters*, *Phys.Lett.* **B673** (2009) 107–110, [[arXiv:0710.1198](#)].
- [39] K. Warnick, A. Knebe, and C. Power, *The Tidal Streams of Disrupting Subhaloes in Cosmological Dark Matter Haloes*, [arXiv:0801.3241](#).
- [40] E. Abdalla, L. R. Abramo, and J. C. de Souza, *Signature of the interaction between dark energy and dark matter in observations*, *Phys.Rev.* **D82** (2010) 023508, [[arXiv:0910.5236](#)].
- [41] J. A. Keselman, A. Nusser, and P. Peebles, *Galaxy Satellites and the Weak Equivalence Principle*, *Phys.Rev.* **D80** (2009) 063517, [[arXiv:0902.3452](#)].
- [42] R. E. Sanderson and E. Bertschinger, *Seen and unseen tidal caustics in the Andromeda galaxy*, *Astrophys.J.* **725** (2010) 1652–1675, [[arXiv:1006.4165](#)].
- [43] K. Benabed and F. Bernardeau, *Testing quintessence models with large scale structure growth*, *Phys.Rev.* **D64** (2001) 083501, [[astro-ph/0104371](#)].
- [44] C.-P. Ma, R. Caldwell, P. Bode, and L.-M. Wang, *The mass power spectrum in quintessence cosmological models*, *Astrophys.J.* **521** (1999) L1–L4, [[astro-ph/9906174](#)].

- [45] E. L. Lokas and Y. Hoffman, *The spherical collapse model in a universe with cosmological constant*, [astro-ph/0011295](#).
- [46] M. Boylan-Kolchin, V. Springel, S. D. White, A. Jenkins, and G. Lemson, *Resolving Cosmic Structure Formation with the Millennium-II Simulation*, *Mon.Not.Roy.Astron.Soc.* **398** (2009) 1150, [[arXiv:0903.3041](#)].
- [47] F. Marulli, M. Baldi, and L. Moscardini, *Clustering and redshift-space distortions in interacting dark energy cosmologies*, *Mon.Not.Roy.Astron.Soc.* **420** (2012) 2377, [[arXiv:1110.3045](#)].
- [48] R. Mainini, A. V. Maccio, and S. Bonometto, *Non-linear predictions from linear theories on models with dark energy*, *New Astron.* **8** (2003) 173–178, [[astro-ph/0207581](#)].
- [49] R. Mainini, A. V. Maccio, S. Bonometto, and A. Klypin, *Modeling dynamical dark energy*, *Astrophys.J.* **599** (2003) 24–30, [[astro-ph/0303303](#)].
- [50] E. L. Lokas, P. Bode, and Y. Hoffman, *Cluster mass functions in the quintessential universe*, *Mon.Not.Roy.Astron.Soc.* **349** (2004) 595, [[astro-ph/0309485](#)].
- [51] P. Solevi, R. Mainini, and S. Bonometto, *The Nature of dark energy from deep cluster abundance*, *Astrophys.J.* (2004) [[astro-ph/0412054](#)].
- [52] P. Solevi, R. Mainini, S. Bonometto, A. Maccio, A. Klypin, et al., *Tracing the nature of dark energy with galaxy distribution*, *Mon.Not.Roy.Astron.Soc.* **366** (2006) 1346–1356, [[astro-ph/0504124](#)].
- [53] M. Manera and D. Mota, *Cluster number counts dependence on dark energy inhomogeneities and coupling to dark matter*, *Mon.Not.Roy.Astron.Soc.* **371** (2006) 1373, [[astro-ph/0504519](#)].
- [54] M. Le Delliou, *Dynamical quintessence fields Press-Schechter mass function: Detectability and effect on dark haloes*, *JCAP* **0601** (2006) 021, [[astro-ph/0506200](#)].
- [55] E. R. Tarrant, C. van de Bruck, E. J. Copeland, and A. M. Green, *Coupled Quintessence and the Halo Mass Function*, *Phys.Rev.* **D85** (2012) 023503, [[arXiv:1103.0694](#)].
- [56] G. Kauffmann, B. Guiderdoni, and S. D. White, *Faint galaxy counts in a hierarchical universe*, *Mon.Not.Roy.Astron.Soc.* **267** (1994) 981.
- [57] C. Baugh, S. Cole, C. Frenk, and C. G. Lacey, *The Epoch of galaxy formation*, *Astrophys.J.* **498** (1998) 504, [[astro-ph/9703111](#)].
- [58] R. S. Somerville and J. R. Primack, *Semianalytic modeling of galaxy formation. The Local Universe*, *Mon.Not.Roy.Astron.Soc.* **310** (1999) 1087, [[astro-ph/9802268](#)].
- [59] S. Cole, C. G. Lacey, C. M. Baugh, and C. S. Frenk, *Hierarchical galaxy formation*, *Mon.Not.Roy.Astron.Soc.* **319** (2000) 168, [[astro-ph/0007281](#)].
- [60] S. Hatton, J. E. Devriendt, S. Ninin, F. R. Bouchet, B. Guiderdoni, et al., *Galics I: a hybrid n-body semi-analytic model of hierarchical galaxy formation*, *Mon.Not.Roy.Astron.Soc.* **343** (2003) 75–106, [[astro-ph/0309186](#)].
- [61] M. Le Delliou, C. Lacey, C. M. Baugh, B. Guiderdoni, R. Bacon, et al., *The abundance of lyman-alpha emitters in hierarchical models*, *Mon.Not.Roy.Astron.Soc.* **357** (2005) L11, [[astro-ph/0405304](#)].
- [62] M. Le Delliou, C. G. Lacey, C. Baugh, and S. Morris, *The Properties of Ly-alpha emitting galaxies in hierarchical galaxy formation models*, *Mon.Not.Roy.Astron.Soc.* **365** (2006) 712–726, [[astro-ph/0508186](#)].
- [63] W. H. Press and P. Schechter, *Formation of galaxies and clusters of galaxies by selfsimilar gravitational condensation*, *Astrophys.J.* **187** (1974) 425–438.
- [64] R. B. Larson, *Numerical calculations of the dynamics of collapsing proto-star*, *Mon.Not.Roy.Astron.Soc.* **145** (1969) 271.

- [65] M. Penston, *Dynamics of self-gravitating gaseous spheres-III. Analytical results in the free-fall of isothermal cases*, *Mon.Not.Roy.Astron.Soc.* **144** (1969) 425.
- [66] J. E. Gunn and I. Gott, J. Richard, *On the Infall of Matter into Clusters of Galaxies and Some Effects on Their Evolution*, *Astrophys.J.* **176** (1972) 1–19.
- [67] J. Fillmore and P. Goldreich, *Self-similar gravitational collapse in an expanding universe*, *Astrophys.J.* **281** (1984) 1–8.
- [68] E. Bertschinger, *The self-similar evolution of holes in an Einstein-de Sitter universe*, *Astrophys.J.Suppl.* **58** (1985) 1.
- [69] P. Peebles, *Large-Scale Structure of the Universe*. Princeton Series in Physics. Princeton University Press, 1980.
- [70] M. Le Delliou, *Self-Similar Infall Models for Dark Matter Haloes*. PhD thesis, Queen’s University, Kingston, Canada, 2001.
- [71] R. Henriksen and M. L. Delliou, *Coarse graining the distribution function of cold dark matter*, *Mon.Not.Roy.Astron.Soc.* **331** (2002) 423, [[astro-ph/0201154](#)].
- [72] M. Le Delliou and R. N. Henriksen, *Non-radial motion and the nfw profile*, *Astron.Astrophys.* **408** (2003) 27–38, [[astro-ph/0307046](#)].
- [73] M. L. Delliou, *Merger is Intermittent Accretion*, *Astron.Astrophys.* **490** (2008) L43–L48, [[arXiv:0705.1144](#)].
- [74] M. Le Delliou, R. N. Henriksen, and J. D. MacMillan, *Black Holes and Galactic Density Cusps Spherically Symmetric Anisotropic Cusps*, *Astron.Astrophys.* **522** (2010) A28, [[arXiv:0911.2234](#)].
- [75] M. Le Delliou, R. N. Henriksen, and J. D. MacMillan, *Black Holes and Galactic Density Cusps : From Black Hole to Bulge*, *Astron.Astrophys.* **526** (2011) A13, [[arXiv:0911.2238](#)].
- [76] M. Le Delliou, R. N. Henriksen, and J. D. MacMillan, *Black Holes and Galactic Density Cusps I Radial Orbit Cusps and Bulges*, *Mon.Not.Roy.Astron.Soc.* **413** (2011) 1633–1642, [[arXiv:0911.2232](#)].
- [77] C. Stubbs, *Experimental limits on any long range nongravitational interaction between dark matter and ordinary matter*, *Phys.Rev.Lett.* **70** (1993) 119–122.
- [78] T. Barreiro, E. J. Copeland, and N. Nunes, *Quintessence arising from exponential potentials*, *Phys.Rev.* **D61** (2000) 127301, [[astro-ph/9910214](#)].
- [79] P. J. Steinhardt, L.-M. Wang, and I. Zlatev, *Cosmological tracking solutions*, *Phys.Rev.* **D59** (1999) 123504, [[astro-ph/9812313](#)].
- [80] P. Brax and J. Martin, *The Robustness of quintessence*, *Phys.Rev.* **D61** (2000) 103502, [[astro-ph/9912046](#)].
- [81] A. Albrecht and C. Skordis, *Phenomenology of a realistic accelerating universe using only Planck scale physics*, *Phys.Rev.Lett.* **84** (2000) 2076–2079, [[astro-ph/9908085](#)].
- [82] R. Mainini and S. A. Bonometto, *Dark matter and dark energy from the solution of the strong-CP problem*, *Phys.Rev.Lett.* **93** (2004) 121301, [[astro-ph/0406114](#)].
- [83] P. G. Ferreira and M. Joyce, *Cosmology with a primordial scaling field*, *Phys.Rev.* **D58** (1998) 023503, [[astro-ph/9711102](#)].
- [84] P. Binetruy, *Models of dynamical supersymmetry breaking and quintessence*, *Phys.Rev.* **D60** (1999) 063502, [[hep-ph/9810553](#)].
- [85] J. P. Mimoso, M. Le Delliou, and F. C. Mena, *Separating expansion from contraction in spherically symmetric models with a perfect-fluid: Generalization of the*

- Tolman-Oppenheimer-Volkoff condition and application to models with a cosmological constant*, *Phys.Rev.* **D81** (2010) 123514, [[arXiv:0910.5755](#)].
- [86] M. Le Delliou, F. C. Mena, and J. P. Mimoso, *The role of shell crossing on the existence and stability of trapped matter shells in spherical inhomogeneous Λ -CDM models*, *Phys.Rev.* **D83** (2011) 103528, [[arXiv:1103.0976](#)].
- [87] M. Le Delliou, J. P. Mimoso, and F. C. Mena, *Trapped matter shell in a perfect fluid ansatz, in preparation* (2012).
- [88] N. Suzuki, D. Rubin, C. Lidman, G. Aldering, R. Amanullah, et al., *The Hubble Space Telescope Cluster Supernova Survey: V. Improving the Dark Energy Constraints Above $z>1$ and Building an Early-Type-Hosted Supernova Sample*, *Astrophys.J.* **746** (2012) 85, [[arXiv:1105.3470](#)].
- [89] E. Di Pietro and J.-F. Claeskens, *Future supernovae data and quintessence models*, *Mon.Not.Roy.Astron.Soc.* **341** (2003) 1299, [[astro-ph/0207332](#)].
- [90] S. Nesseris and L. Perivolaropoulos, *Comparison of the legacy and gold snia dataset constraints on dark energy models*, *Phys.Rev.* **D72** (2005) 123519, [[astro-ph/0511040](#)].
- [91] J. Bond, G. Efstathiou, and M. Tegmark, *Forecasting cosmic parameter errors from microwave background anisotropy experiments*, *Mon.Not.Roy.Astron.Soc.* **291** (1997) L33–L41, [[astro-ph/9702100](#)].
- [92] W. Hu and N. Sugiyama, *Small scale cosmological perturbations: An Analytic approach*, *Astrophys.J.* **471** (1996) 542–570, [[astro-ph/9510117](#)].